AMERICAN SOCIETY FOR MICROBIOLOGY | Journal of Virology®

GENETIC DIVERSITY AND EVOLUTION

The Glycan-Binding Trait of the Sarbecovirus Spike N-Terminal Domain Reveals an Evolutionary Footprint

Hua Guo,[a] Ang Li,[a,b] Hao-Feng Lin,[a,b] Mei-Qin Liu,[a,b] Jing Chen,[a] Ting-Ting Jiang,[a] Bei Li,[a] Yi Wang,[a] Michael C. Letko,[c] Wenjie Peng,[d] Zheng-Li Shi[a]

[a]CAS Key Laboratory of Special Pathogens and Biosafety, Wuhan Institute of Virology, Chinese Academy of Sciences, Wuhan, China
[b]University of Chinese Academy of Sciences, Beijing, China
[c]Paul G. Allen School for Global Health, Washington State University, Pullman, Washington, USA
[d]Key Laboratory of Systems Biomedicine (Ministry of Education), Shanghai Center for Systems Biomedicine, Shanghai Jiao Tong University, Shanghai, China

ABSTRACT The spike protein on sarbecovirus virions contains two external, protruding domains: an N-terminal domain (NTD) with unclear function and a C-terminal domain (CTD) that binds the host receptor, allowing for viral entry and infection. While the CTD is well studied for therapeutic interventions, the role of the NTD is far less well understood for many coronaviruses. Here, we demonstrate that the spike NTD from SARS-CoV-2 and other sarbecoviruses binds to unidentified glycans *in vitro* similarly to other members of the *Coronaviridae* family. We also show that these spike NTD (S-NTD) proteins adhere to Calu3 cells, a human lung cell line, although the biological relevance of this is unclear. In contrast to what has been shown for Middle East respiratory syndrome coronavirus (MERS-CoV), which attaches sialic acids during cell entry, sialic acids present on Calu3 cells inhibited sarbecovirus infection. Therefore, while sarbecoviruses can interact with cell surface glycans similarly to other coronaviruses, their reliance on glycans for entry is different from that of other respiratory coronaviruses, suggesting sarbecoviruses and MERS-CoV have adapted to different cell types, tissues, or hosts during their divergent evolution. Our findings provide important clues for further exploring the biological functions of sarbecovirus glycan binding and adds to our growing understanding of the complex forces that shape coronavirus spike evolution.

IMPORTANCE Spike N-terminal domains (S-NTD) of sarbecoviruses are highly diverse; however, their function remains largely understudied compared with the receptor-binding domains (RBD). Here, we show that sarbecovirus S-NTD can be phylogenetically clustered into five clades and exhibit various levels of glycan binding *in vitro*. We also show that, unlike some coronaviruses, including MERS-CoV, sialic acids present on the surface of Calu3, a human lung cell culture, inhibit SARS-CoV-2 and other sarbecoviruses. These results suggest that while glycan binding might be an ancestral trait conserved across different coronavirus families, the functional outcome during infection can vary, reflecting divergent viral evolution. Our results expand our knowledge on the biological functions of the S-NTD across diverse sarbecoviruses and provide insight on the evolutionary history of coronavirus spike.

KEYWORDS sarbecovirus, SARS-related coronavirus, spike-NTD, glycan-binding property, evolutionary trait

The coronavirus spike glycoprotein (S) mediates viral cell entry, a multistep process consisting of cell-surface attachment, receptor binding and membrane fusion. In general, the S protein can be functionally divided into the S1 and S2 subunits. The S1 subunit binds to the host cell receptor, and the S2 subunit mediates the fusion of viral envelope and host cell endosomal membrane or plasma membrane (1–3). The S1

Editor Tom Gallagher, Loyola University Chicago

Address correspondence to Zheng-Li Shi, zlshi@wh.iov.cn, or Wenjie Peng, wenjiep@sjtu.edu.cn.

The authors declare no conflict of interest.

Received 23 June 2022
Accepted 28 June 2022
Published 19 July 2022

subunit can be further divided into the N-terminal domain (NTD) and C-terminal domain (CTD). For many coronaviruses, including severe acute respiratory syndrome coronavirus-2 (SARS-CoV-2) and Middle East respiratory syndrome coronavirus (MERS-CoV), the S-CTD contains a receptor-binding domain (RBD) that engages with proteinaceous host receptor molecules, angiotensin-converting enzyme 2 (ACE2) and dipeptidyl-peptidase 4 (DPP4), respectively (4–7). Other coronaviruses, such as mouse hepatitis coronavirus (MHV), have been shown to use the S-NTD to engage with their host receptors (8, 9). In addition to proteinaceous receptors, some coronaviruses utilize glycans present on the cell surface to mediate viral entry into the cell: the S-NTD in human coronavirus (HCoV)-OC43 and -HKU1 bind 9-*O*-acetylated sialic acids (9-*O*-Ac sialic acid) (10–12).

Evidence from coronaviruses such as MERS-CoV suggests that viral attachment to specific glycans on the cell surface is critical for viral entry and infection (13). The sialic acid-binding function in transmissible gastroenteritis virus (TGEV) has been suggested to influence viral pathogenicity (14–16), and computational modeling suggests sialic acid binding in SARS-CoV-2 spike may be an immune evasion mechanism (17). Recent studies also propose that sialic acid or 9-*O*-Ac sialic acid of glycoproteins and glycolipids might be served as the host factor for SARS-CoV-2 infection (18–22). However, the functional analysis of this phenotype was not fully assessed in cell culture or animal models, leaving the biological impact unknown. In addition, other studies have shown that the SARS-CoV-2 S-NTD harbors an antigenic site capable of inducing neutralizing antibodies similar to those of the S-RBD (23–28), and high-frequency substitutions and deletions have been found in the NTD region of various SARS-CoV-2 variants of concern (VOCs) during human transmission, suggesting the S-NTD of SARS-CoV-2 also plays a critical function in sarbecovirus biology.

Like the RBD in spike, the S-NTD is also divergent both in length and sequence among different sarbecoviruses (Fig. 1A and B), including the SARS-related coronaviruses (SARSr-CoVs) detected in bats and pangolins: SARS-CoV-2-related coronaviruses RaTG13, RmYN02, and pangolin-CoV-GD/GX and SARS-CoV-1-related coronavirus RsWIV1, RsWIV16, and Rp3 (4, 29–34). Both SARS-CoV-1 and -2 likely emerged from these or other closely related bat and pangolin-derived sarbecoviruses through recombination or adaptive evolution through intermediate hosts (2, 3, 35–37). However, similar to the SARS-CoV-2 S-NTD, the role of the S-NTD in these animal-derived sarbecoviruses remains largely understudied. From an evolutionary perspective, it is still unknown if the sialic acid-binding features for SARS-CoV-2 spike are specific to SARS-CoV-2 or coronavirus adaptation to humans or if this spike property is also retained by other sarbecoviruses.

Previous studies have shown that sarbecovirus RBDs phylogenetically group into at least 4 functionally distinct clades (38, 39). Here, we took a similar approach to the sarbecovirus S-NTD and found that this spike domain can also be divided into its own clades, with distinctions in glycan-binding function. These results shed light on the evolutionary history of the S-NTD in sarbecoviruses as well as the potential inhibitory role for sialic acid during viral entry.

RESULTS

Recombinant sarbecovirus S-NTDs do not hemagglutinate the erythrocytes like other coronaviruses. We constructed a phylogenetic tree based on representative sarbecovirus spike NTD amino acid sequences. Similar to what we have observed with the sarbecovirus spike RBD (38, 39), the S-NTDs display high diversity, sharing 42 to 99% amino acid sequence identities with each other and can be phylogenetically clustered into five clades (Fig. 1A and B). We expressed and purified nine representative S-NTD proteins from the different clades for the function study. Because the S-NTD from some coronaviruses can agglutinate human or rat erythrocytes (14, 40), we performed a standard hemagglutination assay (HA) using the recombinant sarbecovirus S-NTD-Fc proteins. The esterase inactive hemagglutinin-esterase (HE) proteins of bovine coronavirus (BCoV-HE^0) and MERS-CoV S-NTD protein were used as a positive and negative control, respectively. As expected, the MERS-CoV S-NTD failed to agglutinate the erythrocytes (13), while the BCoV-HE^0 protein exhibited a clear effect on the rat red blood

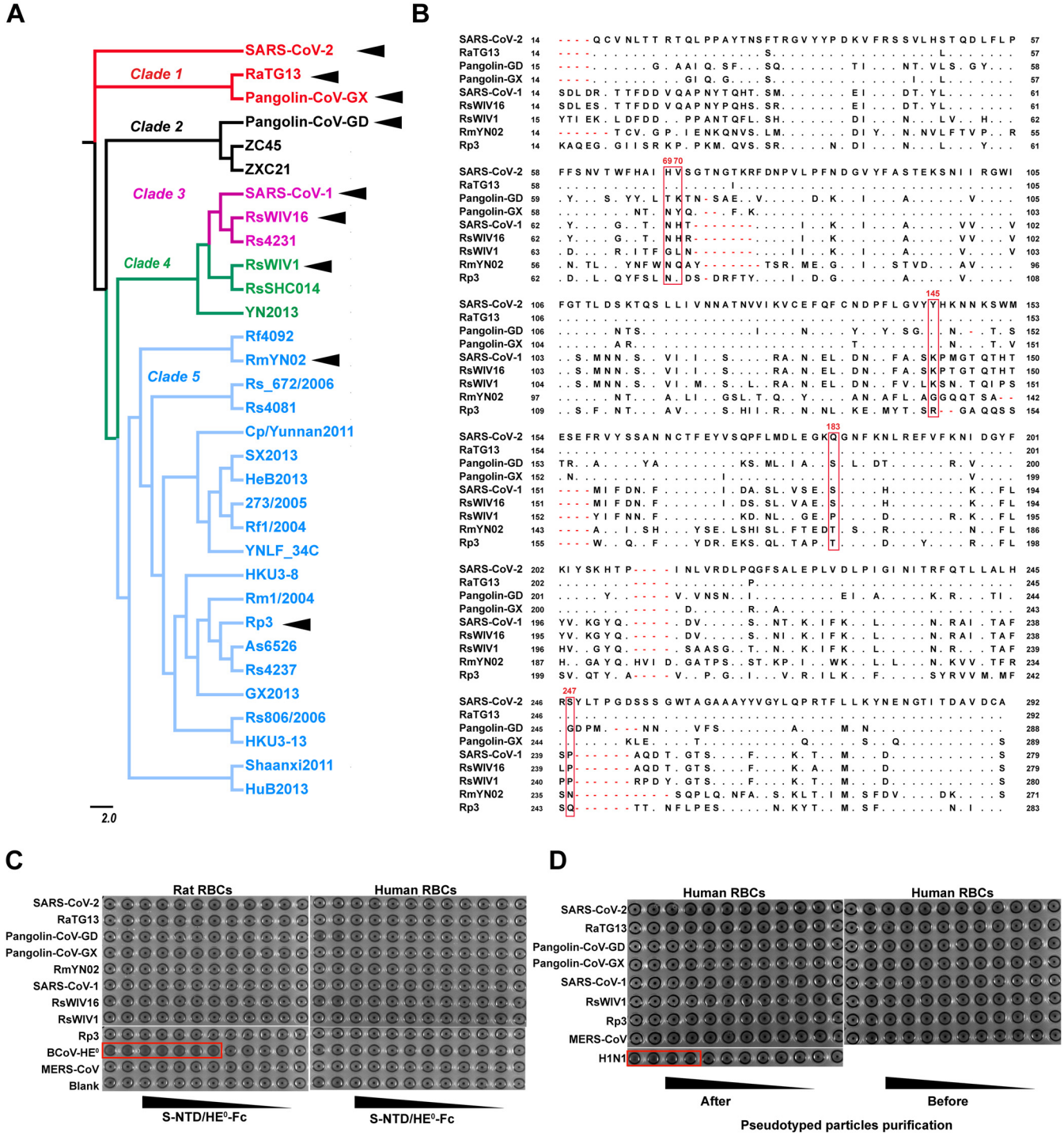

FIG 1 Erythrocyte agglutination test of sarbecovirus S-NTDs. (A) Maximum-likelihood phylogenetic tree of sarbecovirus S-NTD constructed in the RAxML program in CIPRES Science Gateway (https://www.phylo.org) using the Taylor-Thornton (JTT+G+I) model, with bootstrap values determined by 1,000 replicates. (B) Alignment of amino acid sequences of S-NTDs (corresponding to aa14 to 292 of SARS-CoV-2). The red rectangle shows the proposed sialic acid-binding sites in the SARS-CoV-2 spike (19). (C and D) Classical hemagglutination assay. S-NTD/HE^0-Fc proteins (2-fold serial dilutions, starting at 10 μg/well) (C) or coronavirus pseudotyped particles (D) were mixed with RBCs (1%) from humans or rats and then incubated at 4°C for 2 h. Hemagglutination is shown in the red rectangles.

cells (RBCs) (Fig. 1C). We did not observe any hemagglutination for those sarbecovirus S-NTDs in both human and rat erythrocytes, even at higher concentrations of the S-NTD (Fig. 1C). Because purified recombinant S-NTD protein is not truly representative of the multiple spike proteins found on the surface of virus particles, we repeated the

assay using vesicular stomatitis virus (VSV)-based pseudotyped particles bearing different sarbecovirus S proteins in human erythrocytes. Consistent with the results from recombinant S-NTD protein, we did not observe any hemagglutination with sarbecovirus spike pseudotyped particles, even with purified particles (Fig. 1D). In contrast, the positive-control glycoprotein from influenza virus strain H1N1 showed clear hemagglutination (Fig. 1D). These results suggest that sarbecovirus S-NTDs show no or low affinity to glycans, including sialic acids (sialic acid) and ABO blood group antigens.

Sarbecovirus S-NTDs bind to BSM with a wide affinity range *in vitro*. We next tested if the sarbecovirus S-NTDs could interact with other glycans. To start, we measured the affinity between sarbecovirus S-NTD proteins and bovine submaxillary mucin (BSM), which contains glycans that bind to S and HE proteins from several coronaviruses (40–44). BCoV-HE^0, which binds to BSM in a 9-*O*-Ac-Sia-dependent fashion (44), was used as a positive control. Strikingly, we observed that the S-NTDs from clades 1, 2, and 4 and some of the S-NTDs from clade 5 exhibited concentration-dependent binding to BSM, albeit with varied affinities among different clade S-NTDs (Fig. 2A). For example, the S-NTDs from clade 1 showed much higher binding affinity to BSM than pangolin-CoV-GD and RsWIV1, which belong to clade 2 and 4, respectively. Furthermore, the two pangolin-derived SARSr-CoVs, pangolin-CoV-GD (clade 2) and -GX (clade 1), displayed nearly opposite affinities in binding with BSM (Fig. 1A and B, Fig. 2A). The S-NTDs of SARS-CoV-1 and RsWIV16 from clade 3 and bat SARSr-CoV Rp3 in clade 5, as well as the MERS-CoV S-NTD, did not show obvious binding affinity to BSM (Fig. 2A) (13).

To identify ligand molecules in BSM that bind to sarbecovirus S-NTDs, we performed an on-the-plate-*O*-Ac-Sia-depletion assay using pan-active neuraminidase enzymes (NA) from *Clostridium perfringens* (CPN) or *Arthrobacter ureafaciens* (AUS), as well as HE proteins from BCoV and porcine torovirus (PToV), which are esterase-active. The two NAs broadly cleave (α2,6)/(α2,3)/(α2,8)-linked sialic acids, while the two HE proteins convert 7/9-O-Ac modified sialic acid moieties to naive sialic acids (44). Pretreatment of the BSM with the neuraminidases or esterases caused the positive-control protein BCoV-HE^0 to lose its ability to bind with BSM, suggesting both neuraminidases and esterases were enzymatically active. In comparison, neither neuraminidase nor esterase depletion altered the binding properties of sarbecovirus S-NTDs to BSM, except for the pangolin-CoV-GD S-NTD, which showed lower binding affinity to BSM after being treated with *C. perfringens*, but not *A. ureafaciens* (Fig. 2B to D, Fig. 3A).

BSM is a heavily *O*-glycosylated protein rich in (α2,6)-linked 7,9-*O*-Ac sialic acid and 9-*O*-Ac sialic acid (44). The esterase-active HE proteins from BCoV and PToV preferentially cleave the 9-*O*-acetyl group but have lower activity against 7-*O*-acetyl groups (44). The acetyl group at C-7 of sialic acid (Neu5,7Ac$_2$) is unstable and will migrate to C-9 forming Neu5,9Ac$_2$ under physiological conditions or upon pH and temperature changes (45, 46). To further test if the sarbecovirus S-NTDs bind to Neu5,7Ac$_2$ in BSM, we chemically converted the sialosides into Neu5,9Ac$_2$ by treating BSM with 100 mM Tris-HCl (pH = 8.4) at 60°C for 30 min (44), allowing BCoV-HE proteins to cleave the 9-*O* acetyl group of sialic acids. The results showed that none of the S-NTDs abolished the binding affinity to BSM (Fig. 3B).

To test if those glycans are involved in the viral cell entry, we performed a BSM-blocking assay by incubation of pseudovirus or authentic virus with BSM before infecting Calu3 cells. We did not observe significant changes between the treated and nontreated groups (Fig. 2E and F).

Taken together, with the exception of pangolin-CoV-GD S-NTD, most of the tested sarbecovirus S-NTDs do not bind sialic acid regardless of acylation. Moreover, the components of BSM that are bound by S-NTDs may not be involved in the viral entry process.

Sarbecovirus S-NTDs bind to Calu3 cells but are not involved in the viral entry directly. To test if the S-NTDs are involved in viral cell entry, we performed a cell-based binding assay using the Calu3 cell line, which is permissive to sarbecovirus infection and has been reported to contain abundant sialic acids that facilitate MERS-CoV attachment (13). We incubated Calu3 cells with different amounts of S-NTDs and subsequently stained the cells

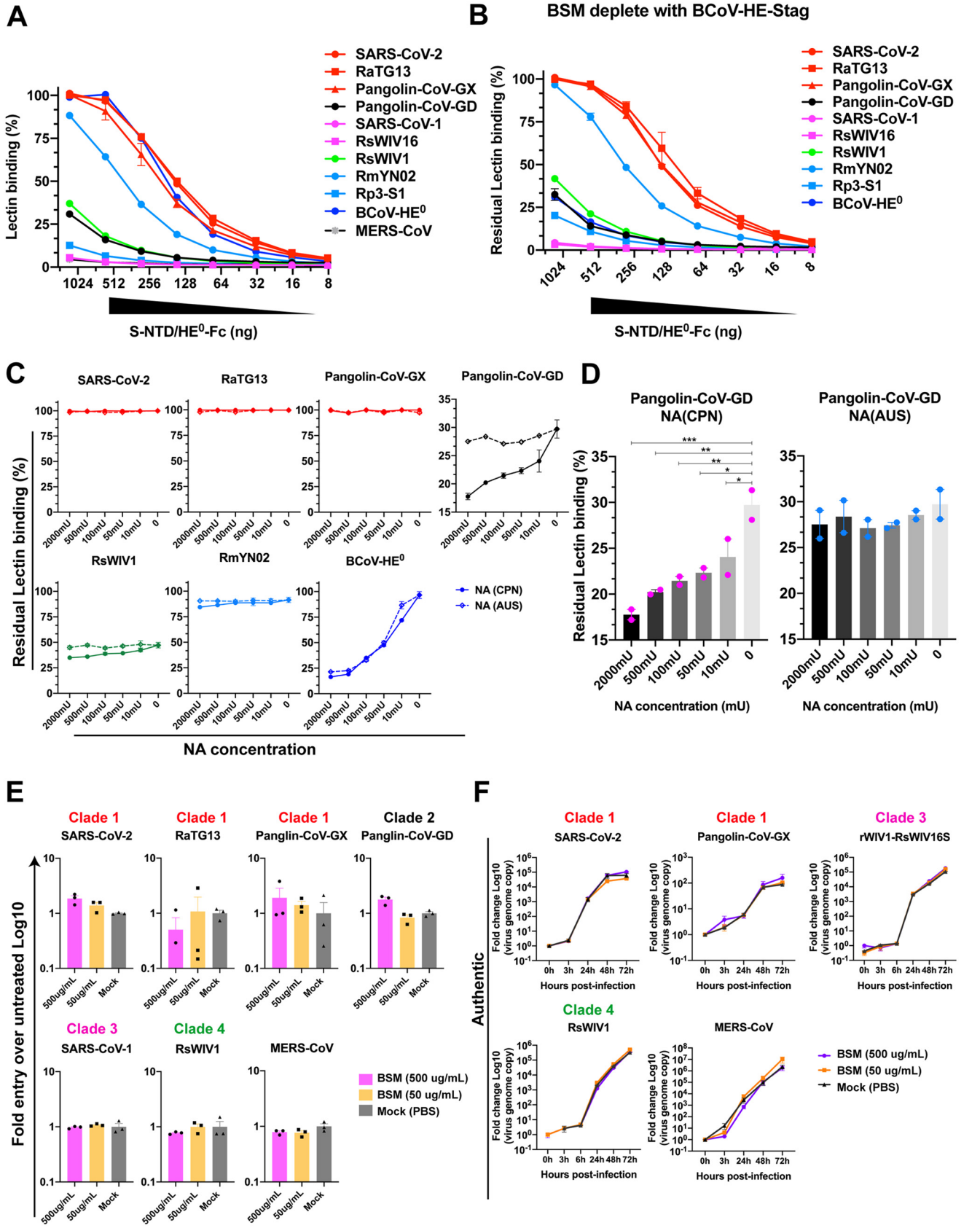

FIG 2 Binding assay between the sarbecovirus S-NTDs and the BSM. (A) SARSr-CoV S-NTDs bind to the glycan molecules in BSM with different affinities. The binding affinities of S-NTD/HE^0-Fc proteins (in 2-fold serial dilutions, starting at 12 ng/μL) to BSM were determined by sp-LBA. (B)

(Continued on next page)

with a fluorescent antibody to detect S-NTD binding by flow cytometry. We observed dose-dependent binding between sarbecovirus S-NTDs and Calu3 cells (Fig. 4A and B). Notably, the sarbecovirus S-NTDs that bound to the Calu3 cells were the same viruses that bound to BSM in our previous experiments (Fig. 2A, Fig. 4B). Furthermore, we found the binding efficiency of SARS-CoV-2 and SARS-CoV-2-related coronavirus S-NTDs to Calu3 cells was much higher than that of SARS-CoV-1, SARS-CoV-1-related coronaviruses, and MERS-CoV (Fig. 4A and B).

Next, we evaluated the impact of S-NTD on viral entry. We incubated Calu3 cells with different amounts of purified S-NTD protein at 37°C for 2 h and subsequently infected them with different pseudoviruses or authentic viruses. The infectivity of the viruses tested was not affected by S-NTDs preincubation (Fig. 4C and D). Taken together, these data indicate that the S-NTD of the sarbecovirus might bind to certain molecules in BSM as well as on the Calu3 cell surface, but the interaction is not critical for virus entry in these assays.

Cleavage of the sialic acids on cell surfaces enhances the sarbecovirus entry. To determine if sialic acids are involved in sarbecovirus viral entry, we treated Calu3 cells with neuraminidase from *Clostridium perfringens* for 2 h at 37°C and then infected the cells with different pseudoviruses. In contrast to our positive control, MERS-CoV, which showed a reduction in entering *C. perfringens*-treated Calu3 cells (13), the entry efficiency of the sarbecovirus displayed significant enhancement after the treatment (Fig. 5A). Because *C. perfringens* treatment reduced binding between pangolin-CoV-GD S-NTD and BSM *in vitro* (Fig. 2C and D), while neuraminidase treatment enhanced viral entry in pseudotype assays, we wondered if our pseudotype stocks were too high in titer for us to observe differences in NTD function. To address this potential artifact, we repeated the infection using serial dilutions of the pangolin-CoV-GD pseudotypes and found that the treatment still increased the entry efficiency of pangolin-CoV-GD regardless of the viral concentration (Fig. 5B).

We then performed a similar infection assay with live viruses, including the original isolate for SARS-CoV-2, pangolin-CoV-GX, and bat SARSr-CoV-1 RsWIV1 and RsWIV16. MERS-CoV was used as the positive control. Viral entry and replication were quantified by measuring viral genome accumulation in the supernatants. Consistent with what we found in the pseudovirus entry assay, *C. perfringens* treatment increased the virus titer in the supernatant of all viruses at 24 h postinfection (hpi). This effect was especially notable for the two bat SARS-CoV-1-related coronaviruses, RsWIV1 and RsWIV16, which showed a continuous increase after 24 h postinfection (hpi) (Fig. 5C). These results are in close agreement with previous findings on SARS-CoV-1 and SARS-CoV-2 (22, 47). Our data suggest that the sialic acids on the surface of the Calu3 cells inhibit entry of sarbecovirus. Together with previous reports, our results demonstrate that this phenomenon may exist in all sarbecoviruses but is dramatically opposite to MERS-CoV.

DISCUSSION

In this study, we explored the function of S-NTD of SARS-CoV-2 as well as other sarbecoviruses in the *Sarbecovirus* subgenus. The five different clades of S-NTD from our phylogenetic analysis exhibited various capabilities of glycan binding, but with less

FIG 2 Legend (Continued)
Esterase depletion assay. BSM was coated on MaxiSorp plates and incubated for 2 h with BCoV-Mebus-HE-Stag protein at fixed concentrations (1.2 μg/well); binding affinities of different S-NTD-Fc proteins to residual O-Ac-sialic acid in BSM were assessed by sp-LBA. Relative binding was compared with BCoV-Mebus-HE^0-Fc proteins in panels A and B (12 ng/μL BCoV-Mebus-HE^0-Fc proteins was set at 100%). (C and D) Neuraminidase depletion assay. BSM-coated MaxiSorp plates were either mock-treated or desialylated by serial concentrations of NA from *Clostridium perfringens* (CPN) and *Arthrobacter ureafaciens* (AUS), followed by incubation with viral S-NTD-Fc protein (C) or pangolin-CoV-GD S-NTD proteins (D). Relative binding was compared with BCoV-Mebus-HE^0-Fc proteins in panels C and D (6 ng/μL BCoV-Mebus-HE^0-Fc protein was set at 100%). All of the binding experiments were performed in duplicate and repeated more than twice. A representative experiment is shown. Error bars represent the mean $\pm$ standard error of the mean (SEM). ***, $P < 0.001$; **, $P < 0.005$; *, $P < 0.05$. (E and F) Impact of BSM on sarbecovirus cell entry in Calu3 cells. SARSr-CoVs pseudovirus (E) or authentic virus (F) stocks were preincubated with 500 μg/mL or 50 μg/mL BSM or PBS at 37°C for 1 h before Calu3 cells were infected. For pseudovirus infection, the data show the relative entry of pseudovirus compared to the mock group. For authentic virus infection, the data show the change of virus genome copy in the supernatant through time in each group compared to 0 h. The above-described infection experiments were performed in duplicate and repeated more than twice. A representative experiment is shown. Error bars represent the mean $\pm$ SEM.

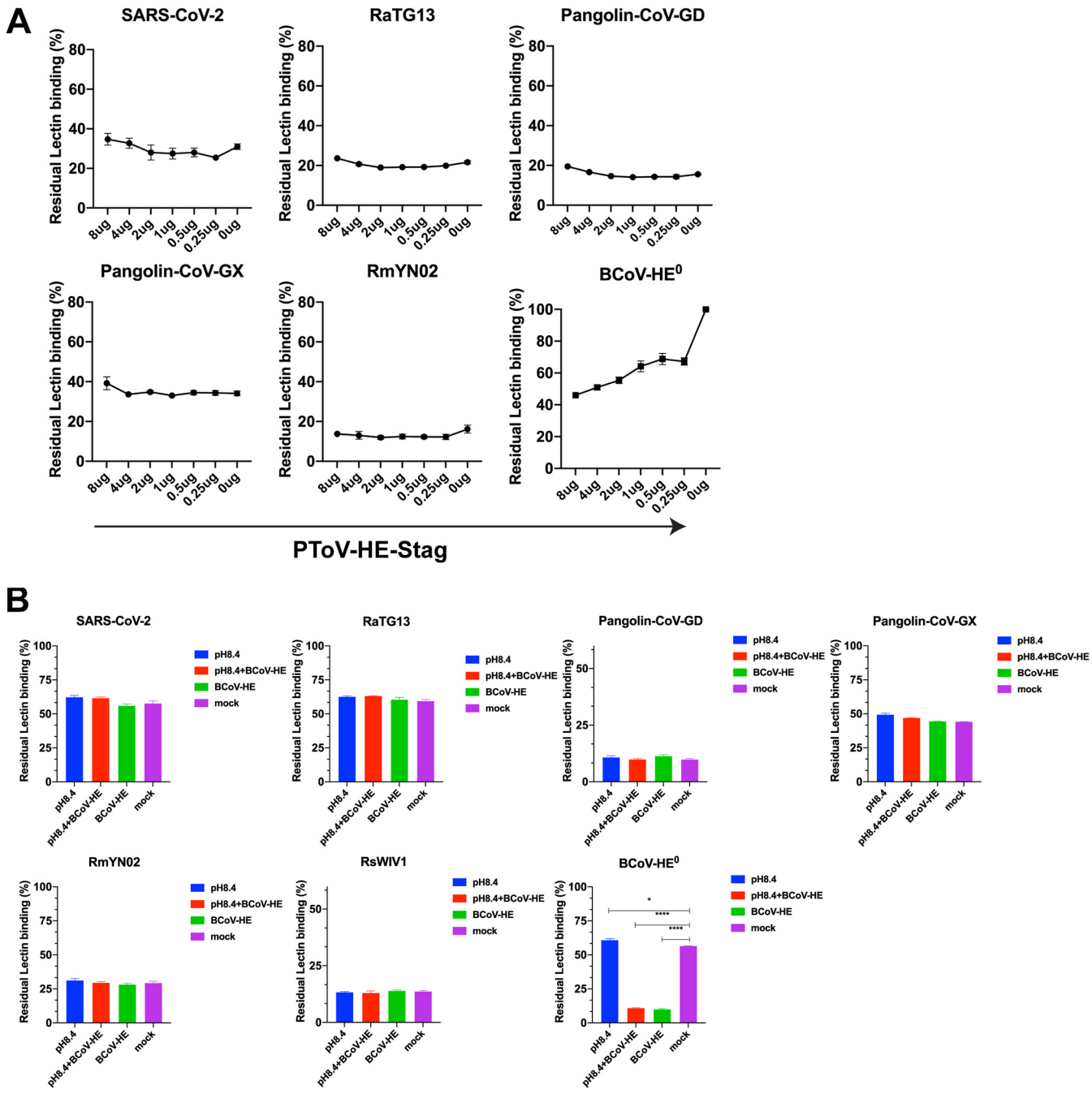

FIG 3 Esterase depletion assay. (A) On-the-plate *O*-Ac-Sia depletion assay. BSM-coated ELISA plates were either mock-treated or de-9-*O*-acetylated by serial concentrations of PToV-HE-Stag protein before incubation with viral S-NTDs. (B) BSM-coated ELISA plates were either mock-treated, de-9-*O*-acetylated using BCoV-HE-Mebus, or induced by migration of the Sia-7-O-acetyl group to C-9 by incubation at 60°C for 30 min with 100 mM Tris-HCl (pH = 8.4) and then mock-treated or treated with BCoV-HE-Mebus before incubation with viral S-NTDs. Relative binding was compared with BCoV-Mebus-HE^0-Fc proteins in panels A and B (6 ng/μL BCoV-Mebus-HE^0-Fc protein was set at 100%). All experiments were performed in duplicate and repeated twice. A representative experiment is shown. Error bars represent the corresponding mean ± SEM. ****, $P < 0.0001$; *, $P < 0.05$.

clear functional delineation than the different clades of RBD that we have defined previously (Fig. 1) (29, 38, 48, 49). While sialic acid removal had a significant positive effect on viral entry and replication for all the sarbecoviruses (Fig. 5), we only observed notable cell adherence for S-NTD from clades 1, 2, and part of clade 5, and purified S-NTD protein had practically no effect on virus infection (Fig. 4). Thus, glycan-binding characteristics might be an ancestral and evolutionary trait of coronaviruses that has been lost or retained during evolutionary history.

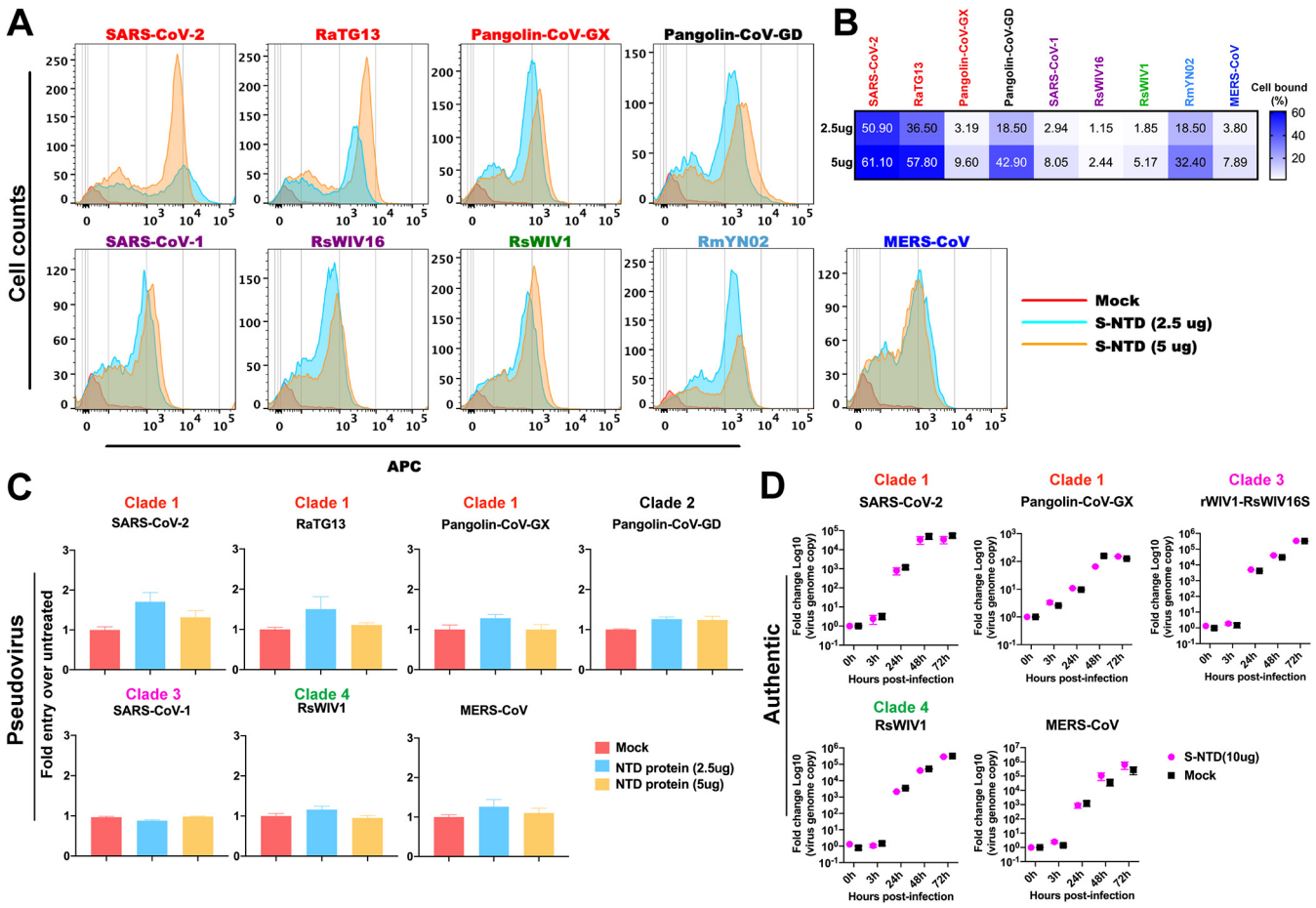

FIG 4 Binding and entry assays of sarbecovirus S-NTDs in Calu3 cells. (A and B) SARSr-CoV S-NTDs bind to Calu3 cells. The Calu3 cells were scraped with a cell scraper and washed twice with PBS before incubation with 2.5 or 5 μg S-NTD proteins at 37°C for 30 min. The binding between S-NTDs and cells was detected by a Dylight650-labeled goat-anti-human IgG Fc antibody. (C and D) SARSr-CoVs S-NTDs preincubated with Calu3 did not affect SARSr-CoVs cell entry. The Calu3 cells were preincubated with different S-NTDs (2.5 or 5 μg for pseudovirus, 10 μg for authentic virus), or PBS before incubation with different pseudovirus (C) or authentic virus (D) stocks. For pseudovirus infection, the data show the relative entry of different SARSr-CoVs compared to the mock (PBS) at 24 hpi. For authentic virus infection, the data show the change of virus genome copy in the supernatant through time in each group compared to 0 h. The above-described experiments were repeated more than twice with three (pseudovirus) or two (authentic virus) technical replicates each time. A representative result is shown. Error bars represent the mean ± SEM.

It is well established that coronaviruses can utilize a diversity of glycan molecules as attachment factors or functional receptors, such as HCoV-OC43, BCoV, and HCoV-HKU1, which engage 9-*O*-Ac-Sia as a receptor (10, 11, 40, 50), that MERS-CoV binds to (α2,3)-linked-sialic acid for attachment (13), and that porcine epidemic diarrhea virus (PEDV) and transmissible gastroenteritis virus (TGEV) have been shown to interact with some sialoglycans during infection (14, 15, 51). Based on the available structural information, the spike residues that bind with saccharides are located within the NTD and are relatively conserved among these viruses (52–54). In this study, we showed that the S-NTD of some sarbecoviruses also binds to certain saccharides in the BSM. Our Sia-depletion assay revealed that the acetylation of the sialic acids, including the 7-*O*, 9-*O*, and 7,9-*O*-acetylated, did not affect the binding of sarbecovirus S-NTDs to BSM (Fig. 2B to D, Fig. 3). In addition, we found that neuraminidase treatment also did not impact the binding of most sarbecovirus S-NTDs to BSM, except for the pangolin-CoV-GD (Fig. 2C and D). A preprint publication showed that the NTD mutations in SARS-CoV-2 variants of concern (VOCs) spike, such as H69, V70, and Y145 in Alpha variants, ablated the sialoside-binding trait of SARS-CoV-2 spike (19). Based on homology studies, we found that the proposed sialic acid-binding sites, including the H69, Q183, and S247 sites in SARS-CoV-2 spike (19), are different from the corresponding amino acids in pangolin-CoV-GD (Fig. 1A), but they are conserved in RaTG13 and pangolin-CoV-GX,

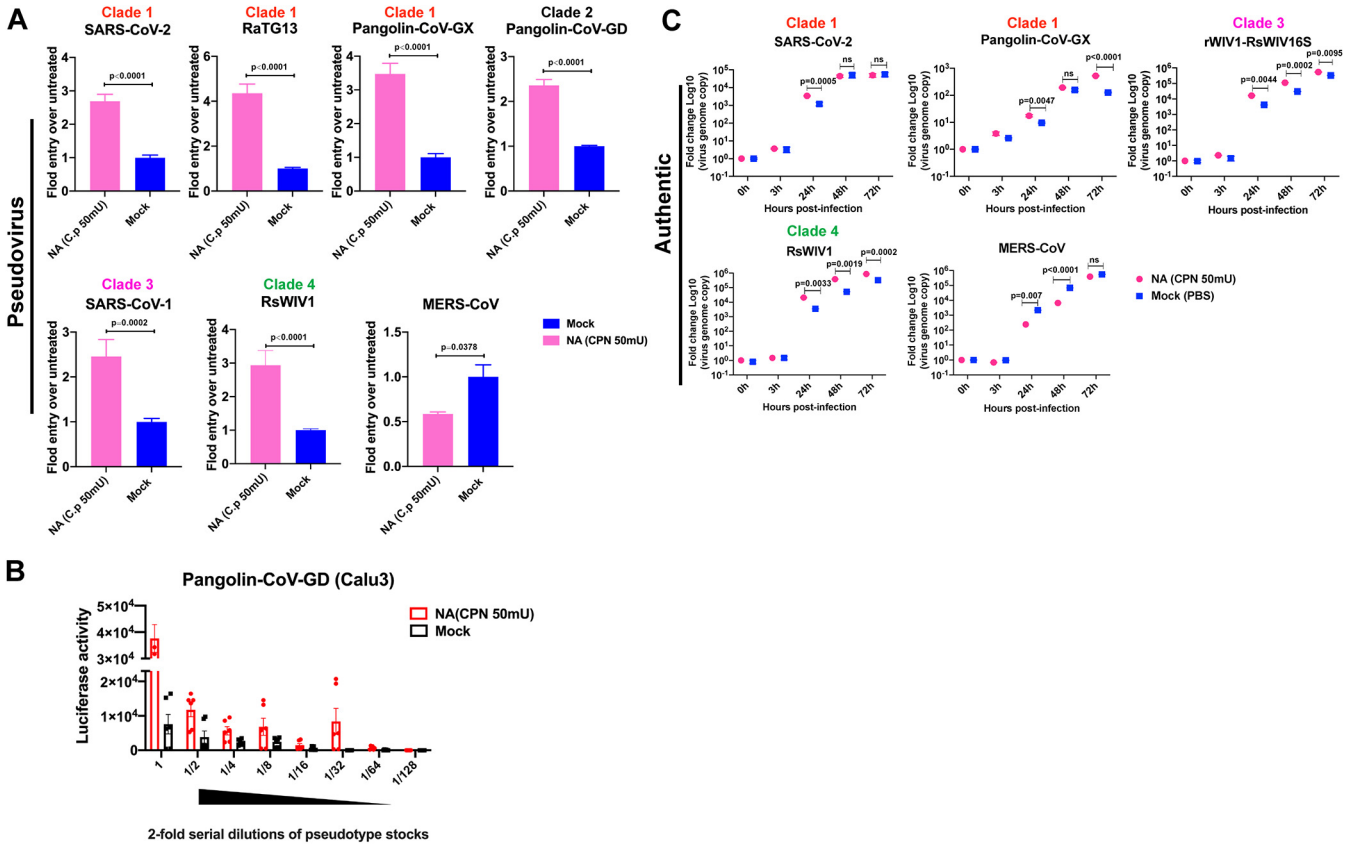

FIG 5 Neuraminidase treatment enhances the cell entry of sarbecovirus. (A to C) Calu3 cells were treated with either 50 mU NA from *C. perfringens* or PBS at 37°C for 2 h before incubation with different pseudovirus (A, B) or authentic virus (C) stocks. For pseudovirus infection, the data show the relative entry of different SARSr-CoVs compared to the mock (PBS) 24 hpi. For authentic virus infection, the data show the change of virus genome copy in the supernatant through time in each group compared to 0 h. The above-described experiments were repeated more than twice with three (pseudovirus) or two (authentic virus) technical replicates each time. A representative result is shown. Error bars represent the mean ± SEM.

which show similar binding affinity to BSM as SARS-CoV-2. These results imply that the topology around the H69, Q183, and S247 sites in sarbecovirus spike may play important roles in binding with saccharides. During the preparation of the manuscript, an NMR study demonstrated that the NTD of SARS-CoV-2 spike binds exogenous (α2,3)/(α2,6)-Neu5Ac linked to *N*-acetyllactosamine, and the galactose moieties display additional contributions for the binding (18). However, in our study, we found neuraminidase cleavage would not abolish the binding of SARS-CoV-2 and other sarbecovirus S-NTDs to BSM. This inconsistency may be caused by the incomplete sialic acid removal in our experiments or the different modifications between Neu5Ac and *N*-glycolyneuraminic acid (Neu5Gc), as the BSM contains both Neu5Ac and Neu5Gc on short *O*-glycans instead of the common *N*-glycans on the cell surface (44). Our results suggest that sarbecovirus may interact with some less-characterized glycan molecules.

Our pseudovirus infection data suggest that neuraminidase pretreatment increases sarbecovirus viral entry in Calu3 cells (Fig. 5A). This result is generally consistent with the previous studies, and the small difference in SARS-CoV-1 and -2 may be caused by the different cell lines and neuraminidase we used in our experiments (22, 47). However, the interfering sialic acids for SARS-CoV-2 are not likely on the viral receptor itself, as blocking O- and N-linked glycan biosynthesis of ACE2 has been shown to have no effect on viral entry or spike binding (55). Recent studies showed that membrane-tethered mucins restrict SARS-CoV-2 infection (56) and that SARS-CoV-2 infection leads to upregulated mucin expression in primary lung epithelial cells (57). Thus, mucins may act as a barrier to protect host cells from infection. In contrast, other viruses, such as influenza A virus (IAV), interact with sialic acid residues as a viral receptor and

subsequently destroy the sialic acids upon egress from the cell to facilitate viral progeny release. A previous study showed that the coinfection of IAV and SARS-CoV-2 enhances SARS-CoV-2 infectivity by upregulating the expression of ACE2 (58). Combining the results from this study, it is possible that the neuraminidase expressed during IAV infection could also increase susceptibility to SARS-CoV-2 infection or enhance disease progression by removal of the sialic acid barrier on cells.

Similar to influenza, which must also overcome sialic acids to exit from the cell, some coronaviruses that are known to use sialic acids for cell entry further encode a receptor-destroying enzyme. The HE enzyme encoded by some coronaviruses helps remove sugar moieties from the cell surface to help with egress, as is well described for the human respiratory virus, HCoV-OC43 (42). The role of sugar binding and the challenges it presents to viral replication are not fully understood for viruses that do not encode HE or use sialic acid as a receptor. For example, while the S-NTD from MERS-CoV has been shown to bind sialic acids, the binding affinity is actually very low and the cells that express abundant DPP4 are typically low in sialoglycan (13). As the virus has evolved, these compromises may allow MERS-CoV to balance virion attachment and progeny release. In this study, we found that neither preincubating Calu3 cells with S-NTDs nor preincubating the virus with BSM make an obvious impact on sarbecovirus cell entry, suggesting that as long as the S-RBD binds to the protein receptor, the glycan-binding method of the sarbecovirus S-NTD may have a minor effect on virus entry. Curiously, these NTDs have maintained a lectin-function domain in their S-NTD, like other coronaviruses, during their evolution. Therefore, future work is required to determine if there is a tissue- or cell-type-specific role for this sugar-binding function, as well as how coronaviruses without esterase enzymes, such as the sarbecoviruses, balance virion attachment and progeny release.

As SARS-CoV-2 circulated globally, high-frequency mutations were observed in the spike NTD of different SARS-CoV-2 VOCs. Despite part of the mutations being shared by different VOCs, most of the mutations appear to occur randomly. One study showed that the mutations in H69 and Y145 in Alpha variant spike abolished its ability to bind sialoside (19). Thus, in humans, the NTD of SARS-CoV-2 spike appears to have a high tolerance to mutations, and potential loss of glycan binding seems to have a negligible effect on replication *in vitro*. In contrast, glycan binding is conserved among sarbecoviruses detected from wildlife, albeit with various binding affinities. These results suggest that glycan binding may be an evolutionary footprint in sarbecovirus history and that SARS-CoV-2 may still be adapting to humans. Whether the continuously occurring mutations in SARS-CoV-2 spike in the future would impact the glycan-binding characteristics still needs further exploration. In addition, recent studies suggested that the SARS-CoV-2 spike NTD affects the metastability of the spike protein, and it is also important for proteolytic fusion activation in the viral cell entry (28, 59). Taken together, the S-NTD is a functionally critical region in the S protein, capable of modulating viral entry and infection. Therefore, further work is required to determine how glycan binding in the S-NTD of sarbecoviruses influences other viral phenotypes, such as antigenic variability, cross-species transmission, and viral infectivity.

MATERIALS AND METHODS

Plasmid construction. The codon-optimized genes encoding the S-NTDs were synthesized by Sangon Biotech (Shanghai, China) and cloned into a modified pCAGGS mammalian expression vector with an mIgkss signal peptide in the N terminus and a human IgG Fc tag in the C terminus followed by a stop codon. The GenBank accession number were listed below: SARS-CoV-2 (spike aa14-292, QHR63260), SARS-CoV-1 (spike aa14-279, AAP30030), RaTG13 (spike aa14-292, QHR63300), pangolin-CoV-GX (spike aa14-289, QIQ54048), pangolin-CoV-GD (spike aa15-288, QIG55945), RmYN02 (spike aa14-271, QPD89843), RsWIV1 (spike aa15-280, AGZ48831), RsWIV16 (spike aa14-279, ALK02457), Rp3 (spike aa16-673, AAZ67052) and MERS-CoV (spike aa19-357, YP_009047204). The ectodomain of BCoV-Mebus HE (spike aa19-377, GenBank accession number: AH010363) and PToV-Markelo HE (spike aa24-393, GenBank accession number: AJ575363) were synthesized and placed into the expression vector with an N-terminal signal peptide and an S-tag as described previously (60). The enzymatically inactive form of BCoV-HE^0-Fc was constructed through site-directed mutagenesis (amino acid 40 Ser to Ala) as described previously (41) and placed into the same expression vector as described above.

Protein expression and purification. HEK293T/17 cells were transiently transfected with different protein expression plasmids using Lipofectamine 3000 (Life Technologies). Then, 6 h posttransfection, the cells were washed with phosphate-buffered saline (PBS) twice and cultured in a fresh 293T FreeStyle expression medium (Life Technologies) at 37°C in a humidified 5% CO_2 incubator. The supernatant was collected at 48 h posttransfection and centrifuged at 4,000 $\times$ *g* for 10 min at 4°C. The clarified supernatant was purified with protein A/G agarose (Thermo Scientific) and eluted with IgG elution buffer (Thermo Scientific). The HE-Stag proteins of BCoV-Mebus and PToV-Markelo were expressed and purified as previously described (60). The purified proteins were buffered with PBS, quantified using a Qubit 2 fluorometer (Thermo Scientific), and then aliquoted and stored at −80°C for further use.

Solid-phase lectin-binding enzyme-linked immune assay (ELISA) and on-the-plate *O*-Ac-Sia-depletion assay. Solid-phase lectin-binding enzyme-linked immune assay (Sp-LBA) was performed as described previously with minor adjustments (41–43). In brief, bovine submaxillary mucin (BSM) (Sigma) was coated overnight on a 96-well ELISA plate (0.5 μg per well) at 4°C. The wells were washed with washing buffer (PBS, 0.05% Tween 20) twice before incubation with blocking buffer (PBS, 0.05% Tween 20, 2% bovine serum albumin) at room temperature (about 25°C) for 1.5 h. Then the wells were washed three times and incubated with 2-fold serial dilutions of S-NTD-Fc or BCoV-HE^0 proteins at 37°C for 1 h. Horseradish peroxidase (HRP)-conjugated goat anti-human IgG antibody (dilution in blocking buffer) was used to detect the binding between S-NTD-Fc proteins and BSM. For the on-the-plate *O*-Ac-Sia depletion assay, the wells were treated with BCoV-HE, PToV-HE, neuraminidase (from *Clostridium perfringens* and *Arthrobacter ureafaciens*, Sigma) or PBS (mock) at 37°C for 2 h before incubation with different S-NTD-Fc proteins.

Pseudovirus production and entry assays. Different coronavirus S-pseudotyped VSV-ΔG particles were generated as previously described with minor adjustments (61, 62). Briefly, HEK 293T/17 cells were transfected with codon-optimized sarbecovirus and MERS-CoV spike plasmids. Then, 24 h posttransfection, the cells were infected with VSV-G-pseudotyped VSV△G/Fluc at 37°C for 1 h and then washed five times with PBS and supplied with fresh Dulbecco's modified Eagle's medium (DMEM) plus 10% fetal bovine serum (FBS) medium plus 1 μg/mL anti-VSV-G antibody (Kerafast). The supernatants were harvested 48 h after infection and centrifuged at 4,000 $\times$ *g* for 10 min at 4°C. The pseudotyped particles were used for infection directly.

The pseudovirus infection assay was performed on Calu3 cell lines. For the neuraminidase treatment assay, the Calu3 cells were incubated with neuraminidase from *Clostridium perfringens* or PBS (mock) at 37°C for 2 h before challenge with different pseudoviruses. For the BSM-blocking assay, the same amount of pseudotyped particles was mock-treated or preincubated with BSM at 37°C for 1 h before infecting the monolayers in a 96-well plate. For the S-NTD blocking assay, the Calu3 cells were incubated with different concentrations of S-NTD proteins (2.5 μg or 5 μg/well) at 37°C for 1 h, followed by different pseudovirus challenges. After 1 to 2 h of incubation, pseudovirus stocks were removed and fresh DMEM/F12 plus 15% FBS medium was to culture for another 24 h. Firefly luciferase expression was measured using a GloMax luminometer (Promega Biotech Co. Ltd., Beijing, China). Infection experiments were performed independently in triplicate with three technical replicates each time. All work with the VSV backbone was conducted under biosafety level 2 conditions.

Virus infection assay. The SARS-CoV-2 strain used in this study was SARS-CoV-2 IVCAS 6.7512 (4), the pangolin-CoV-GX strain was GX/P2V and gifted by Yigang Tong (34), and the bat RsWIV1 and rWIV1-RsWIV16S strains were as previously reported (29, 60). These viruses were grown in Vero E6 cell lines within 3 passages. The MERS-CoV strain used in this study was HCoV-EMC/2012 (GenBank accession number JX869059) and was grown in Vero E6 cell lines. The titer of the virus stocks was determined as previously reported (29). All live virus-related work was conducted under biosafety level 3 conditions. For the neuraminidase treatment assay, the Calu3 cells were incubated with neuraminidase from *Clostridium perfringens* or PBS at 37°C for 2 h before challenge with different virus stocks at a multiplicity of infection (MOI) of 0.1 for 1 h at 37°C. For the S-NTD blocking assay, the Calu3 cells were incubated with 10 μg/well S-NTD proteins at 37°C for 1 h, followed by different virus stock challenges at an MOI of 0.1 for 1 h at 37°C. For the BSM-blocking assay, the virus stocks (MOI = 0.1) were preincubated with different concentrations of BSM (diluted in PBS) or PBS at 37°C for 1 h before infecting the Calu3 cells at 37°C for 1 h. The inoculum was removed after absorption and washed three times with PBS and supplemented with fresh DMEM/F12 plus 15% FBS medium. The viral supernatants were harvested at 0, 3, 24, 48, and 72 hpi and stored at −80°C. The above-described infection assays were performed in a 12-well plate, and 1.5 mL medium per well was used in the cell culture. Infection experiments were independently repeated twice with two technical replicates each time.

Real-time PCR. Viral RNA extraction was performed as previously described (60). The viral replication was determined by quantitative real-time PCR (RT-PCR) using the HiScript II one-step reverse transcription-quantitative PCR (qRT-PCR) SYBR green kit (Q221-01, Vazyme) with the Bio-Rad-CFX system. The primers used for bat RsWIV1, rWIV1-RsWIV16S, and MERS-CoV were as previously reported (60, 63, 64); the primers used for SARS-CoV-2 were SARS-CoV-2-RBD-F, 5′-CAATGGTTTAACAGGCACAGG-3′ and SARS-CoV-2-RBD-R, 5′-CTCAAGTGTCTGTGGATCACG-3′ targeting the spike gene, and the primers used for pangolin-CoV-GX targeting the partial N gene, GX-Np-F, were 5′-ACGTAGTCGCAATAGTTCCAG-3′ and GX-Np-RT-R, 5′-GCATTCAACCGATCAAGCAG-3′. The RNA dilutions from purified RsWIV1 stock which correlated with the threshold cycle (C_T) value and virus titer were used as a standard for bat RsWIV1 and rWIV1-RsWIV16S, and the RNA dilutions from purified SARS-CoV-2 or pangolin-CoV-GX stocks which correlated with the C_T value and virus titer were used as a standard for SARS-CoV-2 and pangolin-CoV-GX, respectively. For MERS-CoV, the N protein gene of MERS-CoV was cloned into the cloning vector as a

plasmid standard, with the viral copy number calculated accordingly. Every sample was analyzed in duplicate on two independent occasions. One representative data set was shown.

Hemagglutination assay. Classical hemagglutination assays were performed as previously reported (65). In brief, the erythrocytes from humans and rats (*Rattus norvegicus* strain Wistar) were suspended in PBS at a final concentration of 1%. The 2-fold serial dilutions of S-NTD-Fc and BCoV HE^0-Fc proteins (starting at 10 μg/well) or pseudotyped particles were incubated with the erythrocytes at 4°C for 2 h.

For the hemagglutination assays using pseudotyped particles, the coronavirus S-pseudotyped VSV-ΔG particles were concentrated through ultracentrifugation. In brief, the culture supernatants containing different coronavirus S-pseudotyped VSV-ΔG particles were loaded onto 2 mL of 20% sucrose in PBS buffer and centrifuged at 30,000 rpm in the SW41 rotor (154,000 × *g*) for 2 h at 4°C (66, 67). The pellets of pseudotyped particles were resuspended in PBS buffer and used for hemagglutination assays directly or stored at −80°C for future use.

ACKNOWLEDGMENTS

We thank Pei Zhang from the core facility of the Wuhan Institute of Virology for her help with the ultracentrifugation. We thank the animal center of the Wuhan Institute of Virology and the core facility of the Wuhan Institute of Virology for their technical support. We also thank Yi-Gang Tong for the generous gift of the pangolin-CoV-GX virus.

The work was jointly supported by the Strategic Priority Research Program of the Chinese Academy of Sciences (XDB29010101 to Z.-L.S.), China Natural National Foundation (31770175 Z.-L.S.), Key Project of Chinese Academy of Sciences (KJZD-SW-L11 to Z.-L.S.), National Science Foundation of China (91853121, 21977066, and 22177069 to W.P.), and Shanghai Pilot Program for Basic Research-Shanghai Jiao Tong University (21TQ1400210 to W.P.).

Z.-L.S. and H.G. conceived the study. H.G. led experimental design. H.G. performed molecular biology experiments. H.G. and A.L. performed BSL-2 experiments. H.-F.L., M.-Q.L., J.C., T.-T.J., and Y.W. performed BSL3 experiments. H.G., A.L., and B.L. performed viral RNA extraction. H.G. analyzed the data and assembled the figures with the help of M.C.L., H.G., M.C.L., W.-J.P., Z.-L.S. wrote the manuscript.

We declare no competing interests.

REFERENCES

1. Masters PS, Perlman S. 2013. Coronaviridae, p 888–922. *In* Knipe DM, Howley PM (ed), Fields virology, 6th ed. Wolters Kluwer, Philadelphia, PA.
2. Jackson CB, Farzan M, Chen B, Choe H. 2022. Mechanisms of SARS-CoV-2 entry into cells. Nat Rev Mol Cell Biol 23:3–20. https://doi.org/10.1038/s41580-021-00418-x.
3. Cui J, Li F, Shi ZL. 2019. Origin and evolution of pathogenic coronaviruses. Nat Rev Microbiol 17:181–192. https://doi.org/10.1038/s41579-018-0118-9.
4. Zhou P, Yang X-L, Wang X-G, Hu B, Zhang L, Zhang W, Si H-R, Zhu Y, Li B, Huang C-L, Chen H-D, Chen J, Luo Y, Guo H, Jiang R-D, Liu M-Q, Chen Y, Shen X-R, Wang X, Zheng X-S, Zhao K, Chen Q-J, Deng F, Liu L-L, Yan B, Zhan F-X, Wang Y-Y, Xiao G-F, Shi Z-L. 2020. A pneumonia outbreak associated with a new coronavirus of probable bat origin. Nature 579:270–273. https://doi.org/10.1038/s41586-020-2012-7.
5. Shang J, Ye G, Shi K, Wan Y, Luo C, Aihara H, Geng Q, Auerbach A, Li F. 2020. Structural basis of receptor recognition by SARS-CoV-2. Nature 581:221–224. https://doi.org/10.1038/s41586-020-2179-y.
6. Walls AC, Park Y-J, Tortorici MA, Wall A, McGuire AT, Veesler D. 2020. Structure, function, and antigenicity of the SARS-CoV-2 spike glycoprotein. Cell 181:281–292.e6. https://doi.org/10.1016/j.cell.2020.02.058.
7. Raj VS, Mou H, Smits SL, Dekkers DH, Muller MA, Dijkman R, Muth D, Demmers JA, Zaki A, Fouchier RA, Thiel V, Drosten C, Rottier PJ, Osterhaus AD, Bosch BJ, Haagmans BL. 2013. Dipeptidyl peptidase 4 is a functional receptor for the emerging human coronavirus-EMC. Nature 495:251–254. https://doi.org/10.1038/nature12005.
8. Shang J, Wan Y, Liu C, Yount B, Gully K, Yang Y, Auerbach A, Peng G, Baric R, Li F. 2020. Structure of mouse coronavirus spike protein complexed with receptor reveals mechanism for viral entry. PLoS Pathog 16:e1008392. https://doi.org/10.1371/journal.ppat.1008392.
9. Williams RK, Jiang GS, Holmes KV. 1991. Receptor for mouse hepatitis virus is a member of the carcinoembryonic antigen family of glycoproteins. Proc Natl Acad Sci U S A 88:5533–5536. https://doi.org/10.1073/pnas.88.13.5533.
10. Huang X, Dong W, Milewska A, Golda A, Qi Y, Zhu QK, Marasco WA, Baric RS, Sims AC, Pyrc K, Li W, Sui J. 2015. Human coronavirus HKU1 spike protein uses O-acetylated sialic acid as an attachment receptor determinant and employs hemagglutinin-esterase protein as a receptor-destroying enzyme. J Virol 89:7202–7213. https://doi.org/10.1128/JVI.00854-15.
11. Krempl C, Schultze B, Herrler G. 1995. Analysis of cellular receptors for human coronavirus OC43. Adv Exp Med Biol 380:371–374. https://doi.org/10.1007/978-1-4615-1899-0_60.
12. Qian Z, Ou X, Goes LG, Osborne C, Castano A, Holmes KV, Dominguez SR. 2015. Identification of the receptor-binding domain of the spike glycoprotein of human betacoronavirus HKU1. J Virol 89:8816–8827. https://doi.org/10.1128/JVI.03737-14.
13. Li W, Hulswit RJG, Widjaja I, Raj VS, McBride R, Peng W, Widagdo W, Tortorici MA, van Dieren B, Lang Y, van Lent JWM, Paulson JC, de Haan CAM, de Groot RJ, van Kuppeveld FJM, Haagmans BL, Bosch B-J. 2017. Identification of sialic acid-binding function for the Middle East respiratory syndrome coronavirus spike glycoprotein. Proc Natl Acad Sci U S A 114:E8508–E8517. https://doi.org/10.1073/pnas.1712592114.
14. Schultze B, Krempl C, Ballesteros ML, Shaw L, Schauer R, Enjuanes L, Herrler G. 1996. Transmissible gastroenteritis coronavirus, but not the related porcine respiratory coronavirus, has a sialic acid (N-glycolylneuraminic acid) binding activity. J Virol 70:5634–5637. https://doi.org/10.1128/JVI.70.8.5634-5637.1996.
15. Schwegmann-Wessels C, Zimmer G, Laude H, Enjuanes L, Herrler G. 2002. Binding of transmissible gastroenteritis coronavirus to cell surface sialoglycoproteins. J Virol 76:6037–6043. https://doi.org/10.1128/jvi.76.12.6037-6043.2002.
16. Schwegmann-Wessels C, Herrler G. 2006. Sialic acids as receptor determinants for coronaviruses. Glycoconj J 23:51–58. https://doi.org/10.1007/s10719-006-5437-9.
17. Li B, Wang L, Ge H, Zhang X, Ren P, Guo Y, Chen W, Li J, Zhu W, Chen W, Zhu L, Bai F. 2021. Identification of potential binding sites of sialic acids on the RBD domain of SARS-CoV-2 spike protein. Front Chem 9:659764. https://doi.org/10.3389/fchem.2021.659764.
18. Unione L, Moure MJ, Lenza MP, Oyenarte I, Ereño-Orbea J, Ardá A, Jiménez-Barbero J. 2022. The SARS-CoV-2 spike glycoprotein directly

binds exogeneous sialic acids: a NMR view. Angew Chem Int Ed Engl 61: e202201432. https://doi.org/10.1002/anie.202201432.
19. Buchanan CJ, Gaunt B, Harrison PJ, Yang Y, Liu J, Khan A, Giltrap AM, Bas AL, Ward PN, Gupta K, Dumoux M, Daga S, Picchiotti N, Baldassarri M, Benetti E, Fallerini C, Fava F, Giliberti A, Koukos PI, Lakshminarayanan A, Xue X, Papadakis G, Deimel LP, Casablancas-Antràs V, Claridge TDW, Bonvin AMJJ, Sattentau QJ, Furini S, Gori M, Huo J, Owens RJ, Schaffitzel C, Berger I, Renieri A, Naismith JH, Baldwin A, Davis BG, GEN-COVID Multicenter Study. 2021. Cryptic pathogen-sugar interactions revealed by universal saturation transfer analysis. bioRxiv https://doi.org/10.1101/2021.04.14.439284.
20. Petitjean SJL, Chen W, Koehler M, Jimmidi R, Yang J, Mohammed D, Juniku B, Stanifer ML, Boulant S, Vincent SP, Alsteens D. 2022. Multivalent 9-O-acetylated-sialic acid glycoclusters as potent inhibitors for SARS-CoV-2 infection. Nat Commun 13:2564. https://doi.org/10.1038/s41467-022-30313-8.
21. Baker AN, Richards S-J, Guy CS, Congdon TR, Hasan M, Zwetsloot AJ, Gallo A, Lewandowski JR, Stansfeld PJ, Straube A, Walker M, Chessa S, Pergolizzi G, Dedola S, Field RA, Gibson MI. 2020. The SARS-COV-2 spike protein binds sialic acids and enables rapid detection in a lateral flow point of care diagnostic device. ACS Cent Sci 6:2046–2052. https://doi.org/10.1021/acscentsci.0c00855.
22. Saso W, Yamasaki M, Nakakita S-i, Fukushi S, Tsuchimoto K, Watanabe N, Sriwilaijaroen N, Kanie O, Muramatsu M, Takahashi Y, Matano T, Takeda M, Suzuki Y, Watashi K. 2022. Significant role of host sialylated glycans in the infection and spread of severe acute respiratory syndrome coronavirus 2. PLoS Pathog 18:e1010590. https://doi.org/10.1371/journal.ppat.1010590.
23. Suryadevara N, Shrihari S, Gilchuk P, VanBlargan LA, Binshtein E, Zost SJ, Nargi RS, Sutton RE, Winkler ES, Chen EC, Fouch ME, Davidson E, Doranz BJ, Chen RE, Shi P-Y, Carnahan RH, Thackray LB, Diamond MS, Crowe JE, Jr. 2021. Neutralizing and protective human monoclonal antibodies recognizing the N-terminal domain of the SARS-CoV-2 spike protein. Cell 184:2316–2331.e15. https://doi.org/10.1016/j.cell.2021.03.029.
24. McCallum M, De Marco A, Lempp FA, Tortorici MA, Pinto D, Walls AC, Beltramello M, Chen A, Liu Z, Zatta F, Zepeda S, di Iulio J, Bowen JE, Montiel-Ruiz M, Zhou J, Rosen LE, Bianchi S, Guarino B, Fregni CS, Abdelnabi R, Foo S-YC, Rothlauf PW, Bloyet L-M, Benigni F, Cameroni E, Neyts J, Riva A, Snell G, Telenti A, Whelan SPJ, Virgin HW, Corti D, Pizzuto MS, Veesler D. 2021. N-terminal domain antigenic mapping reveals a site of vulnerability for SARS-CoV-2. Cell 184:2332–2347.e16. https://doi.org/10.1016/j.cell.2021.03.028.
25. Soh WT, Liu Y, Nakayama EE, Ono C, Torii S, Nakagami H, Matsuura Y, Shioda T, Arase H. 2020. The N-terminal domain of spike glycoprotein mediates SARS-CoV-2 infection by associating with L-SIGN and DC-SIGN. bioRxiv https://doi.org/10.1101/2020.11.05.369264.
26. Liu L, Wang P, Nair MS, Yu J, Rapp M, Wang Q, Luo Y, Chan JFW, Sahi V, Figueroa A, Guo XV, Cerutti G, Bimela J, Gorman J, Zhou T, Chen Z, Yuen K-Y, Kwong PD, Sodroski JG, Yin MT, Sheng Z, Huang Y, Shapiro L, Ho DD. 2020. Potent neutralizing antibodies against multiple epitopes on SARS-CoV-2 spike. Nature 584:450–456. https://doi.org/10.1038/s41586-020-2571-7.
27. Chi X, Yan R, Zhang J, Zhang G, Zhang Y, Hao M, Zhang Z, Fan P, Dong Y, Yang Y, Chen Z, Guo Y, Zhang J, Li Y, Song X, Chen Y, Xia L, Fu L, Hou L, Xu J, Yu C, Li J, Zhou Q, Chen W. 2020. A neutralizing human antibody binds to the N-terminal domain of the spike protein of SARS-CoV-2. Science 369:650–655. https://doi.org/10.1126/science.abc6952.
28. Qing E, Li P, Cooper L, Schulz S, Jäck HM, Rong L, Perlman S, Gallagher T. 2022. Inter-domain communication in SARS-CoV-2 spike proteins controls protease-triggered cell entry. Cell Rep 39:110786. https://doi.org/10.1016/j.celrep.2022.110786.
29. Hu B, Zeng LP, Yang XL, Ge XY, Zhang W, Li B, Xie JZ, Shen XR, Zhang YZ, Wang N, Luo DS, Zheng XS, Wang MN, Daszak P, Wang LF, Cui J, Shi ZL. 2017. Discovery of a rich gene pool of bat SARS-related coronaviruses provides new insights into the origin of SARS coronavirus. PLoS Pathog 13:e1006698. https://doi.org/10.1371/journal.ppat.1006698.
30. Yang XL, Hu B, Wang B, Wang MN, Zhang Q, Zhang W, Wu LJ, Ge XY, Zhang YZ, Daszak P, Wang LF, Shi ZL. 2015. Isolation and characterization of a novel bat coronavirus closely related to the direct progenitor of severe acute respiratory syndrome coronavirus. J Virol 90:3253–3256. https://doi.org/10.1128/JVI.02582-15.
31. Ge X-Y, Li J-L, Yang X-L, Chmura AA, Zhu G, Epstein JH, Mazet JK, Hu B, Zhang W, Peng C, Zhang Y-J, Luo C-M, Tan B, Wang N, Zhu Y, Crameri G, Zhang S-Y, Wang L-F, Daszak P, Shi Z-L. 2013. Isolation and characterization of a bat SARS-like coronavirus that uses the ACE2 receptor. Nature 503: 535–538. https://doi.org/10.1038/nature12711.
32. Zhou H, Chen X, Hu T, Li J, Song H, Liu Y, Wang P, Liu D, Yang J, Holmes EC, Hughes AC, Bi Y, Shi W. 2020. A novel bat coronavirus closely related to SARS-CoV-2 contains natural insertions at the S1/S2 cleavage site of the spike protein. Curr Biol 30:2196–2203.e3. https://doi.org/10.1016/j.cub.2020.05.023.
33. Xiao K, Zhai J, Feng Y, Zhou N, Zhang X, Zou J-J, Li N, Guo Y, Li X, Shen X, Zhang Z, Shu F, Huang W, Li Y, Zhang Z, Chen R-A, Wu Y-J, Peng S-M, Huang M, Xie W-J, Cai Q-H, Hou F-H, Chen W, Xiao L, Shen Y. 2020. Isolation of SARS-CoV-2-related coronavirus from Malayan pangolins. Nature 583:286–289. https://doi.org/10.1038/s41586-020-2313-x.
34. Lam TT-Y, Jia N, Zhang Y-W, Shum MH-H, Jiang J-F, Zhu H-C, Tong Y-G, Shi Y-X, Ni X-B, Liao Y-S, Li W-J, Jiang B-G, Wei W, Yuan T-T, Zheng K, Cui X-M, Li J, Pei G-Q, Qiang X, Cheung WY-M, Li L-F, Sun F-F, Qin S, Huang J-C, Leung GM, Holmes EC, Hu Y-L, Guan Y, Cao W-C. 2020. Identifying SARS-CoV-2-related coronaviruses in Malayan pangolins. Nature 583: 282–285. https://doi.org/10.1038/s41586-020-2169-0.
35. Ruiz-Aravena M, McKee C, Gamble A, Lunn T, Morris A, Snedden CE, Yinda CK, Port JR, Buchholz DW, Yeo YY, Faust C, Jax E, Dee L, Jones DN, Kessler MK, Falvo C, Crowley D, Bharti N, Brook CE, Aguilar HC, Peel AJ, Restif O, Schountz T, Parrish CR, Gurley ES, Lloyd-Smith JO, Hudson PJ, Munster VJ, Plowright RK. 2022. Ecology, evolution and spillover of coronaviruses from bats. Nat Rev Microbiol 20:299–314. https://doi.org/10.1038/s41579-021-00652-2.
36. Andersen KG, Rambaut A, Lipkin WI, Holmes EC, Garry RF. 2020. The proximal origin of SARS-CoV-2. Nat Med 26:450–452. https://doi.org/10.1038/s41591-020-0820-9.
37. Hu B, Guo H, Zhou P, Shi Z-L. 2021. Characteristics of SARS-CoV-2 and COVID-19. Nat Rev Microbiol 19:141–154. https://doi.org/10.1038/s41579-020-00459-7.
38. Letko M, Marzi A, Munster V. 2020. Functional assessment of cell entry and receptor usage for SARS-CoV-2 and other lineage B betacoronaviruses. Nat Microbiol 5:562–569. https://doi.org/10.1038/s41564-020-0688-y.
39. Starr TN, Zepeda SK, Walls AC, Greaney AJ, Alkhovsky S, Veesler D, Bloom JD. 2022. ACE2 binding is an ancestral and evolvable trait of sarbecoviruses. Nature 603:913–918. https://doi.org/10.1038/s41586-022-04464-z.
40. Hulswit RJG, Lang Y, Bakkers MJG, Li W, Li Z, Schouten A, Ophorst B, van Kuppeveld FJM, Boons G-J, Bosch B-J, Huizinga EG, de Groot RJ. 2019. Human coronaviruses OC43 and HKU1 bind to 9-O-acetylated sialic acids via a conserved receptor-binding site in spike protein domain A. Proc Natl Acad Sci U S A 116:2681–2690. https://doi.org/10.1073/pnas.1809667116.
41. Bakkers MJG, Lang Y, Feitsma LJ, Hulswit RJG, de Poot SAH, van Vliet ALW, Margine I, de Groot-Mijnes JDF, van Kuppeveld FJM, Langereis MA, Huizinga EG, de Groot RJ. 2017. Betacoronavirus adaptation to humans involved progressive loss of hemagglutinin-esterase lectin activity. Cell Host Microbe 21:356–366. https://doi.org/10.1016/j.chom.2017.02.008.
42. Lang Y, Li W, Li Z, Koerhuis D, van den Burg ACS, Rozemuller E, Bosch B-J, van Kuppeveld FJM, Boons G-J, Huizinga EG, van der Schaar HM, de Groot RJ. 2020. Coronavirus hemagglutinin-esterase and spike proteins coevolve for functional balance and optimal virion avidity. Proc Natl Acad Sci U S A 117: 25759–25770. https://doi.org/10.1073/pnas.2006299117.
43. Langereis MA, Zeng Q, Heesters BA, Heesters B, Huizinga EG, de Groot RJ. 2012. The murine coronavirus hemagglutinin-esterase receptor-binding site: a major shift in ligand specificity through modest changes in architecture. PLoS Pathog 8:e1002492. https://doi.org/10.1371/journal.ppat.1002492.
44. Langereis MA, Bakkers MJ, Deng L, Padler-Karavani V, Vervoort SJ, Hulswit RJ, van Vliet AL, Gerwig GJ, de Poot SA, Boot W, van Ederen AM, Heesters BA, van der Loos CM, van Kuppeveld FJ, Yu H, Huizinga EG, Chen X, Varki A, Kamerling JP, de Groot RJ. 2015. Complexity and diversity of the mammalian sialome revealed by nidovirus virolectins. Cell Rep 11:1966–1978. https://doi.org/10.1016/j.celrep.2015.05.044.
45. Kamerling JP, Schauer R, Shukla AK, Stoll S, Van Halbeek H, Vliegenthart JFG. 1987. Migration of O-acetyl groups in N,O-acetylneuraminic acids. Eur J Biochem 162:601–607. https://doi.org/10.1111/j.1432-1033.1987.tb10681.x.
46. Barnard KN, Wasik BR, LaClair JR, Buchholz DW, Weichert WS, Alford-Lawrence BK, Aguilar HC, Parrish CR. 2019. Expression of 9-O- and 7,9-O-acetyl modified sialic acid in cells and their effects on influenza viruses. mBio 10:e02490-19. https://doi.org/10.1128/mBio.02490-19.
47. Chu H, Hu B, Huang X, Chai Y, Zhou D, Wang Y, Shuai H, Yang D, Hou Y, Zhang X, Yuen TT-T, Cai J-P, Zhang AJ, Zhou J, Yuan S, To KK-W, Chan IH-Y, Sit K-Y, Foo DC-C, Wong IY-H, Ng AT-L, Cheung TT, Law SY-K, Au W-K, Brindley MA, Chen Z, Kok K-H, Chan JF-W, Yuen K-Y. 2021. Host and viral

determinants for efficient SARS-CoV-2 infection of the human lung. Nat Commun 12:134. https://doi.org/10.1038/s41467-020-20457-w.
48. Guo H, Hu B, Si HR, Zhu Y, Zhang W, Li B, Li A, Geng R, Lin HF, Yang XL, Zhou P, Shi ZL. 2021. Identification of a novel lineage bat SARS-related coronaviruses that use bat ACE2 receptor. Emerg Microbes Infect 10:1507–1514. https://doi.org/10.1080/22221751.2021.1956373.
49. Seifert SN, Bai S, Fawcett S, Norton EB, Zwezdaryk KJ, Robinson J, Gunn B, Letko MC. 2022. An ACE2-dependent Sarbecovirus in Russian bats is resistant to SARS-CoV-2 vaccines. bioRxiv https://doi.org/10.1101/2021.12.05.471310.
50. Schultze B, Herrler G. 1992. Bovine coronavirus uses N-acetyl-9-O-acetylneuraminic acid as a receptor determinant to initiate the infection of cultured cells. J Gen Virol 73:901–906. https://doi.org/10.1099/0022-1317-73-4-901.
51. Liu C, Tang J, Ma Y, Liang X, Yang Y, Peng G, Qi Q, Jiang S, Li J, Du L, Li F. 2015. Receptor usage and cell entry of porcine epidemic diarrhea coronavirus. J Virol 89:6121–6125. https://doi.org/10.1128/JVI.00430-15.
52. Tortorici MA, Walls AC, Lang Y, Wang C, Li Z, Koerhuis D, Boons GJ, Bosch BJ, Rey FA, de Groot RJ, Veesler D. 2019. Structural basis for human coronavirus attachment to sialic acid receptors. Nat Struct Mol Biol 26:481–489. https://doi.org/10.1038/s41594-019-0233-y.
53. Park YJ, Walls AC, Wang Z, Sauer MM, Li W, Tortorici MA, Bosch BJ, DiMaio F, Veesler D. 2019. Structures of MERS-CoV spike glycoprotein in complex with sialoside attachment receptors. Nat Struct Mol Biol 26:1151–1157. https://doi.org/10.1038/s41594-019-0334-7.
54. Peng G, Xu L, Lin YL, Chen L, Pasquarella JR, Holmes KV, Li F. 2012. Crystal structure of bovine coronavirus spike protein lectin domain. J Biol Chem 287:41931–41938. https://doi.org/10.1074/jbc.M112.418210.
55. Yang Q, Hughes TA, Kelkar A, Yu X, Cheng K, Park S, Huang W-C, Lovell JF, Neelamegham S. 2020. Inhibition of SARS-CoV-2 viral entry upon blocking N- and O-glycan elaboration. Elife 9:e61552. https://doi.org/10.7554/eLife.61552.
56. Biering SB, Sarnik SA, Wang E, Zengel JR, Sathyan V, Nguyenla X, Van Dis E, Catamura C, Yamashiro LH, Begeman A, Stark JC, Shon DJ, Fox DM, Puschnik AS, Bertozzi CR, Carette JE, Stanley SA, Harris E, Konermann S, Hsu PD. 2021. Genome-wide, bidirectional CRISPR screens identify mucins as critical host factors modulating SARS-CoV-2 infection. bioRxiv https://doi.org/10.1101/2021.04.22.440848.
57. Liu Y, Lv J, Liu J, Li M, Xie J, Lv Q, Deng W, Zhou N, Zhou Y, Song J, Wang P, Qin C, Tong W-M, Huang B. 2020. Mucus production stimulated by IFN-AhR signaling triggers hypoxia of COVID-19. Cell Res 30:1078–1087. https://doi.org/10.1038/s41422-020-00435-z.
58. Bai L, Zhao Y, Dong J, Liang S, Guo M, Liu X, Wang X, Huang Z, Sun X, Zhang Z, Dong L, Liu Q, Zheng Y, Niu D, Xiang M, Song K, Ye J, Zheng W, Tang Z, Tang M, Zhou Y, Shen C, Dai M, Zhou L, Chen Y, Yan H, Lan K, Xu K. 2021. Coinfection with influenza A virus enhances SARS-CoV-2 infectivity. Cell Res 31:395–403. https://doi.org/10.1038/s41422-021-00473-1.
59. Qing E, Kicmal T, Kumar B, Hawkins GM, Timm E, Perlman S, Gallagher T. 2021. Dynamics of SARS-CoV-2 spike proteins in cell entry: control elements in the amino-terminal domains. mBio 12:e01590-21. https://doi.org/10.1128/mBio.01590-21.
60. Guo H, Hu B-J, Yang X-L, Zeng L-P, Li B, Ouyang S, Shi Z-L. 2020. Evolutionary arms race between virus and host drives genetic diversity in bat severe acute respiratory syndrome-related coronavirus spike genes. J Virol 94:e00902-20. https://doi.org/10.1128/JVI.00902-20.
61. Nie J, Li Q, Wu J, Zhao C, Hao H, Liu H, Zhang L, Nie L, Qin H, Wang M, Lu Q, Li X, Sun Q, Liu J, Fan C, Huang W, Xu M, Wang Y. 2020. Quantification of SARS-CoV-2 neutralizing antibody by a pseudotyped virus-based assay. Nat Protoc 15:3699–3715. https://doi.org/10.1038/s41596-020-0394-5.
62. Johnson MC, Lyddon TD, Suarez R, Salcedo B, LePique M, Graham M, Ricana C, Robinson C, Ritter DG. 2020. Optimized pseudotyping conditions for the SARS-COV-2 spike glycoprotein. J Virol 94:e01062-20. https://doi.org/10.1128/JVI.01062-20.
63. Wang MN, Zhang W, Gao YT, Hu B, Ge XY, Yang XL, Zhang YZ, Shi ZL. 2016. Longitudinal surveillance of SARS-like coronaviruses in bats by quantitative real-time PCR. Virol Sin 31:78–80. https://doi.org/10.1007/s12250-015-3703-3.
64. Lu X, Whitaker B, Sakthivel SKK, Kamili S, Rose LE, Lowe L, Mohareb E, Elassal EM, Al-Sanouri T, Haddadin A, Erdman DD, McAdam AJ. 2014. Real-time reverse transcription-PCR assay panel for Middle East respiratory syndrome coronavirus. J Clin Microbiol 52:67–75. https://doi.org/10.1128/JCM.02533-13.
65. Zeng Q, Langereis MA, van Vliet ALW, Huizinga EG, de Groot RJ. 2008. Structure of coronavirus hemagglutinin-esterase offers insight into corona and influenza virus evolution. Proc Natl Acad Sci U S A 105:9065–9069. https://doi.org/10.1073/pnas.0800502105.
66. Zhang L, Jackson CB, Mou H, Ojha A, Peng H, Quinlan BD, Rangarajan ES, Pan A, Vanderheiden A, Suthar MS, Li W, Izard T, Rader C, Farzan M, Choe H. 2020. SARS-CoV-2 spike-protein D614G mutation increases virion spike density and infectivity. Nat Commun 11:6013. https://doi.org/10.1038/s41467-020-19808-4.
67. Ou X, Liu Y, Lei X, Li P, Mi D, Ren L, Guo L, Guo R, Chen T, Hu J, Xiang Z, Mu Z, Chen X, Chen J, Hu K, Jin Q, Wang J, Qian Z. 2020. Characterization of spike glycoprotein of SARS-CoV-2 on virus entry and its immune cross-reactivity with SARS-CoV. Nat Commun 11:1620. https://doi.org/10.1038/s41467-020-15562-9.